

Xinbo Zhang · Danzi Sun · Wenya Yin · Yujun Chai
Minshou Zhao

The structure and electrochemical characteristics of $\text{La}_{0.67}\text{Mg}_{0.33}(\text{Ni}_{0.8}\text{Co}_{0.1}\text{Mn}_{0.1})_x$ ($x=2.5\text{--}5.0$) multiphase alloys for nickel-metal hydride batteries

Received: 25 October 2004 / Revised: 1 December 2004 / Accepted: 11 March 2005 / Published online: 2 August 2005
© Springer-Verlag 2005

Abstract This paper presents results concerning structure and electrochemical characteristics of the $\text{La}_{0.67}\text{Mg}_{0.33}(\text{Ni}_{0.8}\text{Co}_{0.1}\text{Mn}_{0.1})_x$ ($x=2.5\text{--}5.0$) alloy. It can be found from the result of the Rietveld analyses that the structures of the alloys change obviously with increasing x from 2.5 to 5.0. The main phase of the alloys with $x=2.5\text{--}3.5$ is LaMg_2Ni_9 phase with a PuNi_3 -type rhombohedral structure, but the main phase of the alloys with $x=4.0\text{--}5.0$ is LaNi_5 phase with a CaCu_5 -type hexagonal structure. Furthermore, the phase ratio, lattice parameter and cell volume of the LaMg_2Ni_9 phase and the LaNi_5 phase change with increasing x . The electrochemical studies show that the maximum discharge capacity increases from 214.7 mAh/g ($x=2.5$) to 391.1 mAh/g ($x=3.5$) and then decreases to 238.5 mAh/g ($x=5.0$). As the discharge current density is 1,200 mA/g, the high rate dischargeability (HRD) increases from 51.1% ($x=2.5$) to 83.7% ($x=3.5$) and then decreases to 71.6% ($x=5.0$). Moreover, the exchange current density (I_0) of the alloy electrodes first increases and then decrease with increasing x from 2.5 to 5.0, which is consistent with the variation of the HRD. The cell volume reduces with increasing x in the alloys, which is detrimental to hydrogen diffusion and accordingly decreases the low-temperature dischargeability of the alloy electrodes.

Keywords Crystal structure · High rate dischargeability · Low temperature dischargeability · Exchange current density · Hydrogen diffusion coefficient

Introduction

Due to the shortage of fossil energy and global warming, hydrogen is expected to be a promising energy carrier in the near future. In order for hydrogen to become a viable solution to the energy crisis and environmental problems, storage processes must be improved in terms of specific capacity and security. Among different ways to store hydrogen, absorption in solid is very attractive since it allows safe storage at pressure and temperature close to ambient conditions [1]. There are many kinds of metals and alloys that are able to absorb large quantities of hydrogen and they are used in many fields, such as heat pump, thermal storage system, fuel cell, nickel-metal hydride (Ni–MH) rechargeable battery, and so on.

In recent years, Ni–MH secondary battery, in which hydrogen storage alloy is employed as negative electrode material, has been widely adopted in various portable electronic devices, electric hand tools, and electric vehicles because of its high reversible energy storage density, fast electrochemical activation, long cyclic stability, good charge/discharge kinetics and environmental compatibility [2–7]. To date, almost all commercial Ni–MH batteries are employing AB_5 -type alloys as negative electrode material because of their good overall electrode properties [8]. However, the electrochemical capacity of the AB_5 -type alloys is limited by the single CaCu_5 -type hexagonal structure [9], the energy densities of the Ni–MH batteries are not competing favorably with some other advanced secondary batteries. Therefore, newer type alloys with higher energy density, faster activation, better rate dischargeability and lower cost are urgently needed to replace the conventional rare earth-based AB_5 -type alloys [10].

X. Zhang (✉) · W. Yin · Y. Chai · M. Zhao
Key Laboratory of Rare Earth Chemistry and Physics,
Changchun Institute of Applied Chemistry,
Graduate School of Chinese Academy of Sciences,
Changchun, 130022, People's Republic of China
E-mail: eboat@ciac.jl.cn
Tel.: +86-431-5262365

D. Sun
State Key Laboratory of Electroanalytical Chemistry,
Changchun Institute of Applied Chemistry,
Graduate School of Chinese Academy of Sciences,
Changchun, 130022, People's Republic of China

Recently, Kadir et al. [11–13] have reported the discovery of a new type of ternary alloys with the general formula of RMg_2Ni_9 (R: rare earth, Ca, Y) with PuNi_3 type structure. It is found that some of the R–Mg–Ni based ternary alloys can absorb–desorb 1.8–1.87 wt.% H_2 and are, thus, regarded as promising candidates for reversible gaseous hydrogen storage [14, 15]. As to their electrochemical hydrogen storage, Chen et al. [7] have studied the structure and electrochemical characteristics of $\text{LaCaMg}(\text{NiM})_9$ ($M = \text{Al, Mn}$) alloys, and almost at the same time, Kohno et al. [4] have reported that the discharge capacity of $\text{La}_{0.7}\text{Mg}_{0.3}\text{Ni}_{2.8}\text{Co}_{0.5}$ alloy reached 410 mAh/g, with fairly good cycling stability within 30 cycles. However, up to now only very few studies have been devoted to the evaluation of the electrochemical properties of La–Mg–Ni–Co–Mn system alloys to provide useful information for the further development of this new group of alloys [16].

In this work, on the basis of our previous studies and the belief that the nonstoichiometry may result in some noticeable modification [17], the structure and electrochemical characteristics of the $\text{La}_{0.67}\text{Mg}_{0.33}(\text{Ni}_{0.8}\text{Co}_{0.1}\text{Mn}_{0.1})_x$ ($x = 2.5, 3.0, 3.5, 4.0, 4.5, 5.0$) alloys have been investigated systematically.

Experimental details

Alloy preparation and X-ray diffraction analysis

All alloy samples were prepared by arc-melting carefully the constituent elements or master alloy on a water-cooled copper hearth under argon atmosphere followed by annealing in vacuum for 20 h at 770 K. A slight Mg over composition was needed in order to compensate for the evaporative loss of Mg under reaction conditions. Several attempts were made until the optimum preparative conditions were found. The purity of the metals, i.e., La, Mg, Ni, Co and Mn is higher than 99.9 mass%. The samples were all inverted and remelted five times to ensure good homogeneity. Thereafter, the ingot was crushed first and then ground in mortar mechanically. The resulting powder was captured between sieves of 200 mesh and 300 mesh.

Crystallographic characteristics of the hydrogen storage alloys were investigated by X-ray diffraction (XRD) on Rigaku D/Max 2500PC X-ray diffractometer ($\text{Cu } K_\alpha$ radiation, Bragg-Brentano geometry, 2θ range 10–100°, step size 0.02°, 4 sec/step, backscattered rear graphite monochromator) using JADE5 software [18]. The instrument is calibrated using silicon as standard reference materials before collecting the XRD data.

Electrochemical measurement

The preparation of the disk-type electrodes, the setup of the electrochemical cell and the measurement of electrochemical properties were similar as described in our previous paper [19].

Pressure-composition isotherms (P–C–T) curves were electrochemically obtained by converting the equilibrium potential of the metal hydride electrode to the equilibrium pressure of hydrogen on the basis of Nernst equation using electrochemical data [20] as reported in the reference [21]. The equilibrium potential curves were obtained by alternating the following two processes: (1) a pulse discharge of (25 mA/g × 0.25 h), and (2) a rest period until the potential became almost constant. The equilibrium potential change of approximately 30 mV corresponds to the equilibrium pressure change by one order of magnitude. Since the measured potentials have an error of 1–2 mV, the calculated pressure values are accurate to be within 10% [21].

To evaluate HRD (in the range of 60–1,200 mA g^{-1}), discharge capacities of the alloy electrode at different discharge current densities were measured. The high rate dischargeability HRD (%) was defined as $C_n \times 100 / (C_n + C_{60})$, where C_n was the discharge capacity n mA/g ($n = 60, 240, 480, 720, 960, 1,200$), C_{60} was the additional capacity measured subsequently at 60 mA/g after C_n was measured.

For investigating the electrocatalytic activity of the hydrogen electrode reaction, the linear polarization curves of the electrode were plotted on a EG&G PARC's Model 273 Potentiostat/Galvanostat station by scanning the electrode potential at the rate of 0.1 mV/s from –5 to 5 mV (versus open circuit potential) at 50% depth of discharge (DOD) at 298 K. The polarization resistance R_p can be obtained from the slope of the linear polarization curves. Moreover, the exchange current density (I_0), which is a measure of the catalytic activity of electrode, was calculated from the slopes of polarization curves by the following equation [22],

$$I_0 = \frac{RT}{FR_p}$$

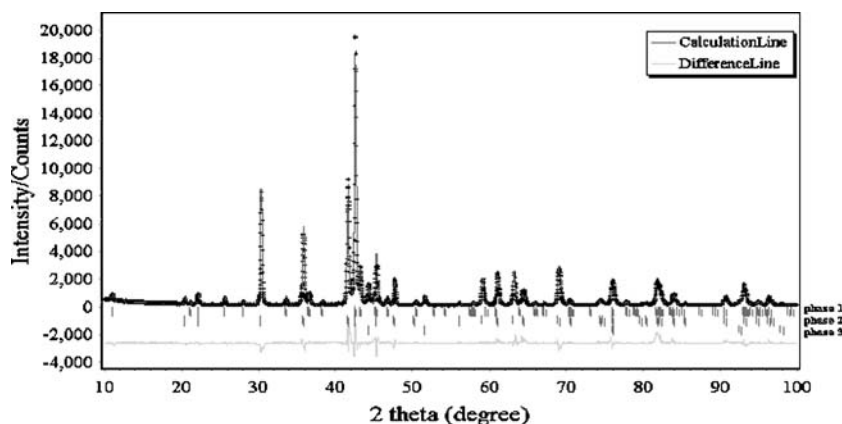
where R is the gas constant; T is the absolute temperature; F is the Faraday constant; and R_p is the polarization resistance. The potentiostatic discharge technique was used to evaluate the coefficient of diffusion within the bulk of the alloy electrodes. After being fully charged followed by a 30-min open-circuit lay-aside, the test electrodes were discharged with +500 mV potential-step for 500 s on a EG&G PARC's Model 273 Potentiostat/Galvanostat station, using the M352 CorrWare electrochemical/corrosion software.

Results and discussion

Structure characteristic

X-ray diffraction and Rietveld method [23, 24] are used to characterize the microstructure, measure the lattice parameters, and verify the phase composition of the $\text{La}_{0.67}\text{Mg}_{0.33}(\text{Ni}_{0.8}\text{Co}_{0.1}\text{Mn}_{0.1})_x$ ($x = 2.5–5.0$) hydrogen storage alloys. Figure 1 shows the Rietveld analysis

Fig. 1 Rietveld profiles refinement of XRD patterns $\text{La}_{0.67}\text{Mg}_{0.33}(\text{Ni}_{0.8}\text{Co}_{0.1}\text{Mn}_{0.1})_4$ alloy (Phase 1: LaMg_2Ni_9 ; phase 2: LaNi_5 ; phase 3: Ni)



patterns of the $\text{La}_{0.67}\text{Mg}_{0.33}(\text{Ni}_{0.8}\text{Co}_{0.1}\text{Mn}_{0.1})_4$ hydrogen storage alloy as an representative example of the $\text{La}_{0.67}\text{Mg}_{0.33}(\text{Ni}_{0.8}\text{Co}_{0.1}\text{Mn}_{0.1})_x$ ($x = 2.5-5.0$) alloys. The final crystallographic parameter of the pseudo- LaMg_2Ni_9 phase (Ni is partially substituted by Co and Mo) is tabulated in Table 1. It can be seen that the substitution of Co and Mo for Ni remains the crystal structure of LaMg_2Ni_9 alloy, i.e., pseudo- LaMg_2Ni_9 phase is isostructural with RMg_2Ni_9 ($R = \text{La, Ce, Pr, Nd, Sm and Gd}$) structure [25], described by the space group $R-3m$ (166) and $Z = 3$. This is consistent with the results of Liu et al. [10]. For the convenience of discussion, LaMg_2Ni_9 phase is employed to represent the pseudo- LaMg_2Ni_9 phase in this work. The lattice parameter, cell volume, and phase ratio of the $\text{La}_{0.67}\text{Mg}_{0.33}(\text{Ni}_{0.8}\text{Co}_{0.1}\text{Mn}_{0.1})_x$ ($x = 2.5-5.0$) alloys are presented in Table 2. It can be found that, besides small amounts of impurity phases (LaNi_2 , LaNi or Ni), all the alloys are composed of a LaMg_2Ni_9 phase with a PuNi_3 -type rhombohedral structure and a LaNi_5 phase with a CaCu_5 -type hexagonal structure. Figure 2 shows the dependence of lattice parameter and unit cell volume of the LaMg_2Ni_9 phase and the LaNi_5 phase on x in the alloys. It can be found that A and cell volume of the LaMg_2Ni_9 phase and the LaNi_5 phase in the alloys decrease monotonically with the increase of x , which might be attributed to the reasons as follows: On the one hand, the atomic ratio of B (B denotes Ni, Co, and Mo) to A

(A represents La and Mg) increases with the increasing x in the alloys, and this would cause increasing defect in the structure, some B atoms would occupy the interstices of the crystal structure. On the other hand, the atomic radius of La (1.877 Å) and Mg (1.72 Å) are all somewhat larger than that of Ni (1.246 Å), Co (1.253 Å) and Mn (1.366 Å). Figure 3 shows the ratio of the LaMg_2Ni_9 phase and the LaNi_5 phase as a function of x in the alloys. As can be seen in Fig. 3 and Table 2, when $x = 2.5, 3.0$ and 3.5 , the main phase of the alloys is LaMg_2Ni_9 phase. However, when x increases from 4.0 to 5.0 progressively, the main phase becomes LaNi_5 phase. Moreover, it can be seen that the LaMg_2Ni_9 phase ratio first remains high and increase from 56.6% to 73.6% and then decreases markedly with increasing x . In contrast, the LaNi_5 phase ratio first remains low and then increase to a high percentage ($> 70\%$) with x increasing from 4.0 to 5.0. These results may influence the hydrogen storage and electrochemical characteristics of the alloys studied.

P-C isotherms

The electrochemical pressure-composition isotherms method is very useful for examining the charging and discharging levels of hydrogen in an anode, although the calculated pressures pertain to a quasi-equilibrium state

Table 1 Crystallographic parameter for pseudo- LaMg_2Ni_9 by using X-ray diffraction (XRD) $\text{Cu K}\alpha$ ($\lambda = 1.5405981 \text{ \AA}$) at 298 K in a space group $R-3m$ and $Z = 3$

Structure was refined by using the Rietveld refinement program Rietica. The pattern factor $R_p = 7.9$, the weighted pattern factor $R_{wp} = 10.7$ and the goodness of fit $\text{GoF} = 2.6$

Atom	Site	Metal atom position			Occupancy
		x	y	z	
La	3a	0	0	0	1
Mg	6c	0	0	0.14754(13)	1
Ni1	6c	0	0	0.32559(15)	0.781
Ni2	3b	0	0	0.5	0.784
Ni3	18h	0.4948(1)	0.5049(9)	0.08342(7)	0.768
Co1	6c	0	0	0.32559(15)	0.106
Co2	3b	0	0	0.5	0.111
Co3	18h	0.4948(1)	0.5049(9)	0.08342(7)	0.115
Mo1	6c	0	0	0.32559(15)	0.113
Mo2	3b	0	0	0.5	0.105
Mo3	18h	0.4948(1)	0.5049(9)	0.08342(7)	0.117

Table 2 Characteristics of alloy phases in $\text{La}_{0.67}\text{Mg}_{0.33}(\text{Ni}_{0.8}\text{Co}_{0.1}\text{Mn}_{0.1})_x$ ($x=2.5, 3.0, 3.5, 4.0, 4.5, 5.0$) alloys

Samples	Phases	Phase ratio (wt. %)	Parameters of fit ^a	Lattice parameter (Å)			Cell volume (Å ³)
				a	b	c	
$x=2.5$	LaMg_2Ni_9	56.6	$R_p=8.8$	5.082	5.082	24.495	547.87
	LaNi_5	33.3	$R_{wp}=11.6$	5.049	5.049	3.983	87.93
	LaNi_2	10.1	$\text{GoF}=2.7$	7.251	7.251	7.41	381.2
$x=3.0$	LaMg_2Ni_9	65.6	$R_p=10$	5.06	5.06	24.389	540.79
	LaNi_5	24.2	$R_{wp}=13.7$	5.027	5.027	3.976	87.02
	LaNi	0.2	$\text{GoF}=2.8$	3.83	11.006	4.468	188.34
$x=3.5$	LaMg_2Ni_9	73.6	$R_p=9.9$	5.041	5.041	24.298	534.73
	LaNi_5	26.3	$R_{wp}=13.1$	5.023	5.023	3.973	86.81
	LaNi	0.1	$\text{GoF}=2.8$	3.854	10.846	4.365	182.46
$x=4.0$	LaMg_2Ni_9	26.4	$R_p=7.9$	5.03	5.03	24.245	531.24
	LaNi_5	73.5	$R_{wp}=10.7$	5.018	5.018	3.968	86.53
	Ni	0.1	$\text{GoF}=2.6$	3.559	3.559	3.559	45.08
$x=4.5$	LaMg_2Ni_9	20.2	$R_p=5.6$	4.986	4.986	24.033	517.42
	LaNi_5	79.5	$R_{wp}=7.5$	5.006	5.006	3.963	86.01
	Ni	0.3	$\text{GoF}=1.8$	3.542	3.542	3.542	44.44
$x=5.0$	LaMg_2Ni_9	8.4	$R_p=8.7$	4.951	4.951	23.864	506.59
	LaNi_5	83.5	$R_{wp}=11.4$	5.002	5.002	3.965	85.91
	Ni	8.1	$\text{GoF}=2.7$	3.533	3.533	3.533	44.1

The Rietveld refinement program RIETICA [24] was used

^a R_p : the pattern factor, R_{wp} : the weighted pattern factor; GoF : the goodness of fit

[26]. The P-C-T curves for hydrogen desorption in the $\text{La}_{0.67}\text{Mg}_{0.33}(\text{Ni}_{0.8}\text{Co}_{0.1}\text{Mn}_{0.1})_x\text{-H}$ system at 298 K are presented in Fig. 4. With the increase of x , the plateau pressure of the alloys increases continuously. The characteristic of the pressure plateau of the hydrogen storage alloy can be mainly ascribed to two reasons: On the one

hand, it is well known that unit cell of the AB_3 compounds contains one-third AB_5 and two-third AB_2 structure [7] and thus, the plateau pressure of the LaMg_2Ni_9 phase is similar to that of LaNi_5 phase. On the other hand, the cell volume of both the LaMg_2Ni_9 phase and the LaNi_5 phase decreases with increasing x , as shown in Table 2 and Fig. 2, which increases the plateau pressure of the hydrogen storage alloy. The hydrogen storage capacity of the alloys is shown in Table 3. It can be seen that, with the increase of x in the alloys, the hydrogen storage capacity increases first and achieves its maximum value ($\text{H}/\text{M}=0.989$) as $x=3.5$, and then decreases to a much low value ($\text{H}/\text{M}=0.583$). This may be attributed to that the relative change of the phase ratio of the LaMg_2Ni_9 phase and LaNi_5 phase in the alloys. As seen in Table 2 and Fig. 3, with the

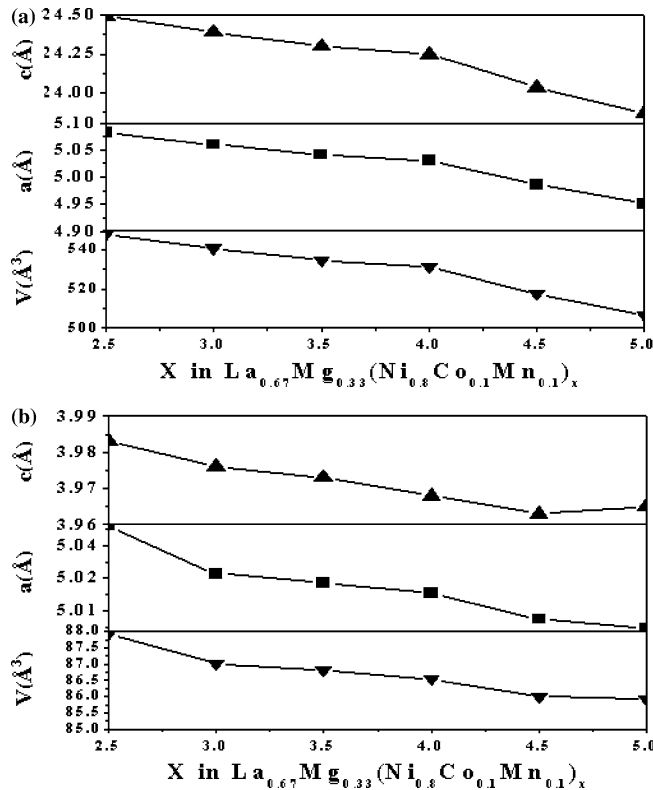


Fig. 2 Lattice parameters and cell volume of the $\text{La}_{0.67}\text{Mg}_{0.33}(\text{Ni}_{0.8}\text{Co}_{0.1}\text{Mn}_{0.1})_x$ ($x=2.5, 3.0, 3.5, 4.0, 4.5, 5.0$) alloys **a** LaMg_2Ni_9 phase **b** LaNi_5 phase

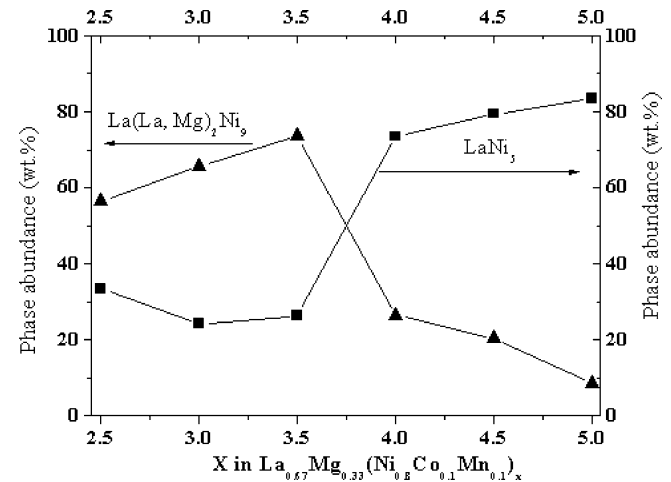
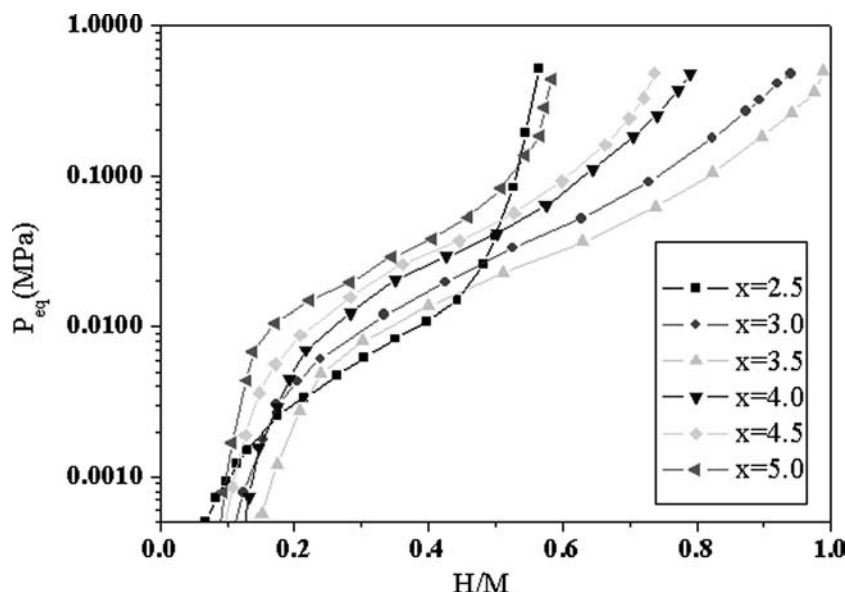


Fig. 3 Phase abundance of the $\text{La}(\text{La}, \text{Mg})_2\text{Ni}_9$ phase and the LaNi_5 phase existing in the $\text{La}_{0.67}\text{Mg}_{0.33}(\text{Ni}_{0.8}\text{Co}_{0.1}\text{Mn}_{0.1})_x$ ($x=2.5, 3.0, 3.5, 4.0, 4.5, 5.0$) alloys

Fig. 4 The electrochemical desorption P-C-T curves for $\text{La}_{0.67}\text{Mg}_{0.33}(\text{Ni}_{0.8}\text{Co}_{0.1}\text{Mn}_{0.1})_x$ ($x = 2.5, 3.0, 3.5, 4.0, 4.5, 5.0$) alloys at 298 K



increase of x , the ratio of the LaMg_2Ni_9 phase increases first and then decreases, in contrast, the ratio of the LaNi_5 phase decreases initially and then increases continuously. Oesterreicher et al. [27] and Takeshita et al. [28] have pointed out that the hydrogen storage capacity of LaNi_3 with PuNi_3 -type structure exceeded that of the well-known LaNi_5 alloys. This lends credence to our assumption that the change of hydrogen storage capacity for the alloys results from the relative variation of the phase ratio of the LaMg_2Ni_9 phase and LaNi_5 phase.

Activation, maximum discharge capacity and cycle stability

Figure 5 shows the cyclic life curves of the $\text{La}_{0.67}\text{Mg}_{0.33}(\text{Ni}_{0.8}\text{Co}_{0.1}\text{Mn}_{0.1})_x$ ($x = 2.5-5.0$) alloy electrodes. It can be seen that all the alloy electrodes can be fully activated within four charge/discharge cycles. The maximum discharge capacities of the alloy electrodes are summarized in Table 3. With the increase of x , the maximum discharge capacity of the alloy electrode first

increase from 214.7 mAh/g ($x = 2.5$) to 391.1 mAh/g ($x = 3.5$) and then decreases to 238.5 mAh/g ($x = 5.0$), which is in good agreement with the results of P-C-T curves measurement. The cycling capacity retention rate, expressed as $S_{70} (\%) = C_{70}/C_{\text{max}} \times 100$ (where C_{max} is the maximum discharge capacity, C_{70} is the discharge capacity at the 70th cycles), after 70 cycles at 60 mA/g is also listed in Table 3. As shown in Fig. 5 and Table 3, it is found that the capacity retention rate (S_{70}) of the alloy electrodes is not changed obviously ($S_{70} = 52.9-54.4\%$), indicating that their cycling stability is rather poor and hence has to be upgraded for practical applications.

High-rate dischargeability

Figure 6 shows the effect of the discharge current density on the discharge capacity of the $\text{La}_{0.67}\text{Mg}_{0.33}(\text{Ni}_{0.8}\text{Co}_{0.1}\text{Mn}_{0.1})_x$ ($x = 2.5-5.0$) alloy electrodes. It can be seen that the HRD of all the alloys decreases monotonously with the increase in the discharge current density. Taking the discharge current density being 1,200 mA/g as an example, the HRD of the alloy electrodes are listed in Table 3, it can be easily seen that the HRD of the alloy electrodes increases from 51.1% ($x = 2.5$) to 83.7% ($x = 3.5$) and then decreases to 71.6% ($x = 5.0$). This phenomenon is in good agreement with the results previously reported by Pan et al. [29]. It is generally accepted that the high-rate dischargeability of a metal-hydride electrode is mainly determined by the charge-transfer process occurring at the metal electrolyte interface or/and the hydrogen diffusion process in the hydride bulk [30, 31]. From the linear polarization curves of the alloy electrodes, the polarization resistance R_p and exchange current density I_0 are obtained and listed in Table 4. It can be seen that the polarization resistance R_p of the alloy electrodes decreases from 299.49 m Ω /g ($x = 2.5$) to 98.86 m Ω /g ($x = 3.5$) and then

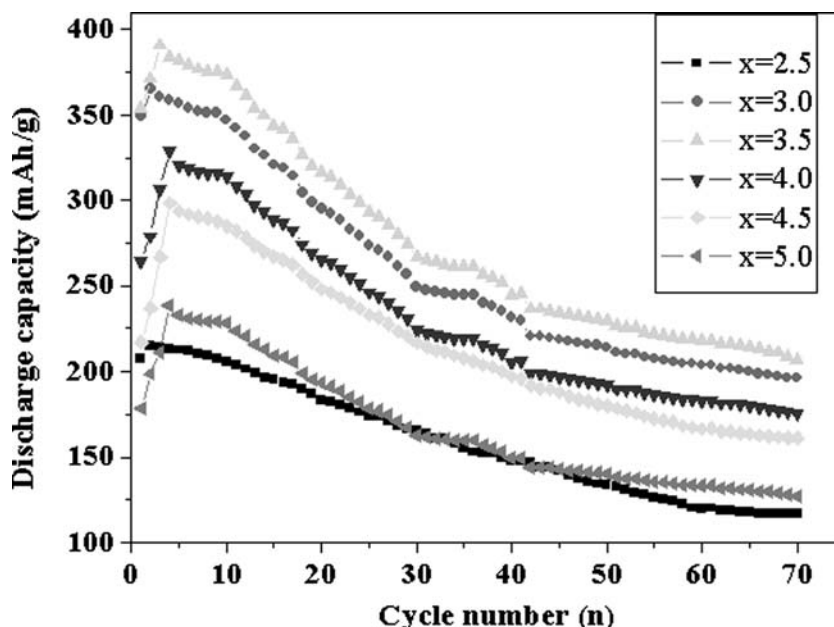
Table 3 Electrode performance of $\text{La}_{0.67}\text{Mg}_{0.33}(\text{Ni}_{0.8}\text{Co}_{0.1}\text{Mn}_{0.1})_x$ ($x = 2.5, 3.0, 3.5, 4.0, 4.5, 5.0$) alloy electrodes

Samples	H/M	C_{max} (mAh/g)	N_a^a	HRD $_{1,200}^b$ (%)	S_{70} (%)
$x = 2.5$	0.565	214.7	2	51.1	54.4
$x = 3.0$	0.941	365.3	2	72.6	53.7
$x = 3.5$	0.989	391.1	3	83.7	52.9
$x = 4.0$	0.82	328.7	4	79.5	53.4
$x = 4.5$	0.736	298.6	4	77.7	54
$x = 5.0$	0.583	238.8	4	71.6	53.2

^aThe cycle numbers needed to activated the electrodes

^bThe high rate dischargeability at the discharge current density of 1,200 mA/g

Fig. 5 The cycle life curves of the $\text{La}_{0.67}\text{Mg}_{0.33}(\text{Ni}_{0.8}\text{Co}_{0.1}\text{Mn}_{0.1})_x$ ($x = 2.5, 3.0, 3.5, 4.0, 4.5, 5.0$) alloy electrodes at 298 K



increases to 127.31 mΩ/g ($x = 5.0$), accordingly the exchange current density I_0 of the alloy electrodes increases from 92.3 to 259.8 mA/g when x increases from 2.5 to 3.5 and then decreases to 184.9 mA/g with x further increasing to 5.0. As shown in Fig. 7, the high-rate dischargeability shows a linear relationship with the exchange density I_0 for the alloy electrodes with $x = 2.5$ –5.0, suggesting that the high-rate dischargeability of the alloy electrodes is essentially controlled by the charge-transfer reaction of the hydrogen at the discharge rate of 1,200 mA/g.

Low-temperature dischargeability (LTD)

It has been reported that the discharge capacity of the negative electrode in nickel-metal hydride decrease

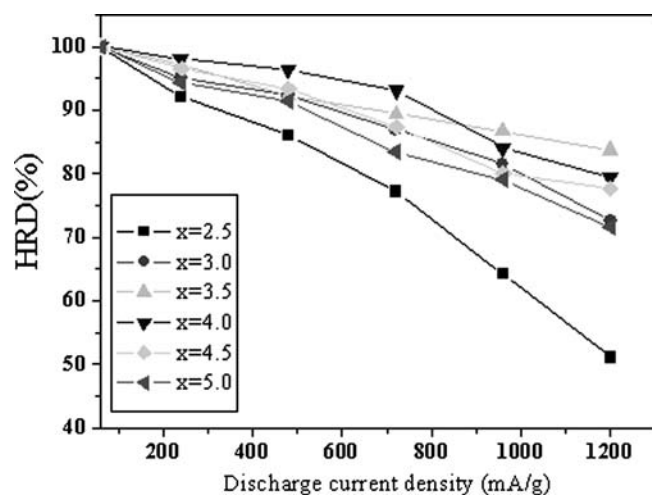


Fig. 6 The high rate dischargeability (HRD) of the $\text{La}_{0.67}\text{Mg}_{0.33}(\text{Ni}_{0.8}\text{Co}_{0.1}\text{Mn}_{0.1})_x$ ($x = 2.5, 3.0, 3.5, 4.0, 4.5, 5.0$) alloy electrodes at 298 K

drastically with decreasing temperature [32]. Sakai et al. [33] reported that the dischargeability of the negative electrodes at relative low temperature depended on the hydrogen diffusion. The LTD, expressed as $\text{LTD}_{233}(\%) = C_{233}/C_{298} \times 100$ (where C_{233} and C_{298} are the discharge capacity at 233 K and 298 K, respectively). Figure 8 shows the LTD as a function of D in the alloy electrodes. It can be easily found that the D decreases with the increases of x , which can be attributed to the cell volume reduction with increasing x as shown in Table 2. The increasing D accordingly decreases the LTD of the alloy electrodes.

Conclusion

The effect of compositions on the structure and electrochemical characteristics of the $\text{La}_{0.67}\text{Mg}_{0.33}(\text{Ni}_{0.8}\text{Co}_{0.1}\text{Mn}_{0.1})_x$ ($x = 2.5, 3.0, 3.5, 4.0, 4.5, 5.0$) alloys has been studied systematically. The results of the Rietveld analyses show that the structures of the alloys change obviously with increasing x from 2.5 to 5.0. The main phase of the alloys with $x = 2.5$ –3.5 is LaMg_2Ni_9 phase with a PuNi_3 -type rhombohedral structure, but the

Table 4 The electrochemical kinetic parameters of $\text{La}_{0.67}\text{Mg}_{0.33}(\text{Ni}_{0.8}\text{Co}_{0.1}\text{Mn}_{0.1})_x$ ($x = 2.5, 3.0, 3.5, 4.0, 4.5, 5.0$) alloy electrodes

Samples	Polarization resistance ^a , R_p (mΩ/g)	Exchange current density ^a , I_0 (mA/g)	Hydrogen diffusion coefficient ^b , D ($\times 10^{-11}$ cm ² /s)
$x = 2.5$	299.49	78.6	14.65
$x = 3.0$	141.45	181.5	13.73
$x = 3.5$	98.86	259.8	12.94
$x = 4.0$	107.69	238.3	11.42
$x = 4.5$	111.89	210.4	9.51
$x = 5.0$	127.31	184.9	7.32

^aObtained at 298 K

^bEvaluated at 233 K

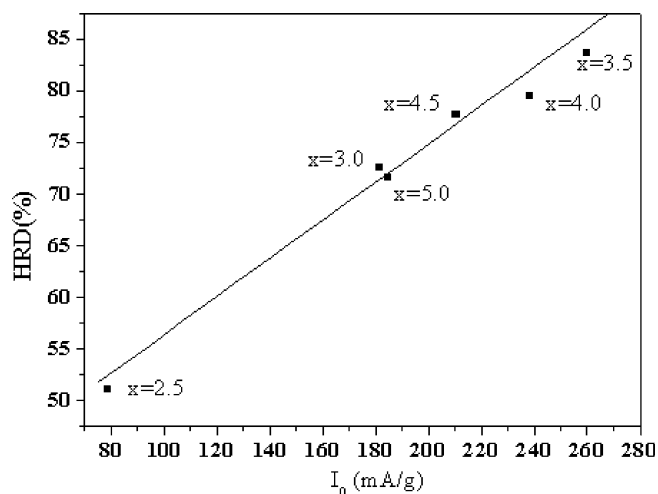


Fig. 7 High rate dischargeability (HRD) at 1,200 mA/g as a function of exchange current density I_0 for $\text{La}_{0.67}\text{Mg}_{0.33}(\text{Ni}_{0.8-x}\text{Co}_{0.1}\text{Mn}_{0.1})_x$ ($x=2.5, 3.0, 3.5, 4.0, 4.5, 5.0$) alloy electrodes

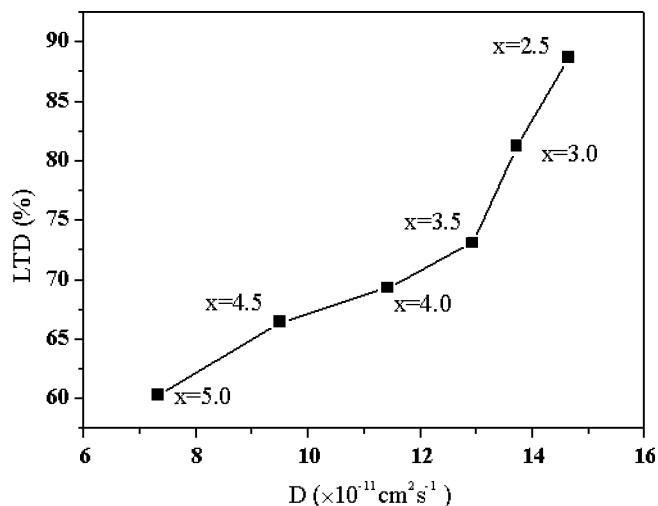


Fig. 8 The low-temperature dischargeability as a function of hydrogen diffusion coefficient of the $\text{La}_{0.67}\text{Mg}_{0.33}(\text{Ni}_{0.8-x}\text{Co}_{0.1}\text{Mn}_{0.1})_x$ ($x=2.5, 3.0, 3.5, 4.0, 4.5, 5.0$) alloy electrodes at 233 K

main phase of the alloys with $x=4.0\text{--}5.0$ is LaNi_5 phase with a CaCu_5 -type hexagonal structure. Moreover, the phase ratio, lattice parameter and cell volume of the LaMg_2Ni_9 phase and the LaNi_5 phase change with increasing x . The electrochemical studies show that the maximum discharge capacity increases from 214.7 mAh/g ($x=2.5$) to 391.1 mAh/g ($x=3.5$) and then decreases to 238.5 mAh/g ($x=5.0$). As the discharge current density is 1,200 mA/g, the HRD increases from 51.1% ($x=2.5$) to 83.7% ($x=3.5$) and then decreases to 71.6% ($x=5.0$). Furthermore, the exchange current density of the alloy electrodes first increases and then decrease with increasing x from 2.5 to 5.0, which is consistent with the variation of the HRD. The cell volume reduces with increasing x , which is detrimental

to hydrogen diffusion and accordingly decreases the low-temperature dischargeability of the alloy electrodes.

Acknowledgements This work was financially supported by the National Natural Science Foundation of China (Grant No.20171042).

References

1. Latroche M, Percheron-Guegan A (2003) *J Alloys Comp* 461:356–357
2. Willems JJG, Buschow KHJ (1987) *J Less-Common Met* 13:129
3. Sakai T, Miyamura H, Kuriyama N, Kato A, Oguro K, Ishikawa H (1990) *J Electrochem Soc* 795:137
4. Kohno T, Yoshida H, Kawashima F, Inaba T, Sakai I, Yamamoto M, Kanda M (2000) *J Alloys Comp* L5:311
5. Willems JJG (1984) *Philips J Res* 39(Suppl 1):1
6. Pan HG, Zhu YF, Gao MX, Wang QD (2002) *J Electrochem Soc* A829:149
7. Chen J, Kuriyama N, Takeshita HT, Tanaka H, Sakai T, Haruta M (2000) *Electrochem Solid State Lett* 3(6):249
8. Sakai T, Uehara I, Iwakura H (1999) *J Alloys comp* 762:293–295
9. Reilly JJ, Adzic GD, Johnson JR, Vogt T, Mukerjee S, McBreen J (1999) *J Alloys Comp* 569:293–295
10. Liu YF, Pan HG, Gao MX, Li R, Lei YQ (2004) *J Alloys Comp* 296:376
11. Kadir K, Sakai T, Uehara I (1997) *J Alloys Comp* 115:257
12. Kadir K, Nuriyama N, Sakai T, Uehara I, Eriksson L (1999) *J Alloys Comp* 145:284
13. Kadir K, Sakai T, Uehara I (1999) *J Alloys Comp* 264:287
14. Kadir K, Sakai T, Uehara I (2000) *J Alloys Comp* 112:302
15. Chen J, Takeshita HT, Tanaka H, Kuriyama N, Sakai T (2000) *J Alloys Comp* 304:302
16. Liao B, Lei YQ, Chen LX, Lu GL, Pan HG, Wang QD (2004) *J Power Sources* 358:129
17. Zhang XB, Zhao MS (2003) *Chem J Chinese U* 24(9):1680
18. Materials Data JADE Release 5 (1997) XRD pattern processing. Materials Data Inc (MDI)
19. Zhang XB, Chai YJ, Yin WY, Zhao MS (2004) *J Solid State Chem* 2373:177
20. Balej J (1985) *Int J Hydrogen Energy* 365:10
21. Iwakura C, Asaoka T, Yoneyama H, Sakai T, Oguro K, Ishikawa H (1988) *Nippon Kagaku Kaishi* 1482
22. Notten PHL, Hokkeling P (1991) *J Electrochem Soc* 1877:138
23. Young RA (1993) *The Rietveld method*. Oxford University Press, Oxford
24. Howard C J (1982) *J Appl Cryst* 615:15
25. Kadir K, Sakai T, Uehara I (1997) *J Alloys Comp* 115:257
26. Sakai T, Miyamura H, Kuriyama N, Kato A, Oguro K, Ishikawa H (1990) *J Less Common Met* 127:159
27. Chen J, Kuriyama N, Takeshita HT, Tanaka H, Sakai T, Haruta M (2000) *Electrochem Solid State Lett* 3(6):249
28. Oesterreicher H, Clinton J, Bittner H (1976) *Mater Res Bull* 1241:11
29. Takeshita T, Wallace WE, Craig RS (1974) *Inorg Chem* 2282:13
30. Pan HG, Liu YF, Gao MX, Zhu YF, Lei YQ (2003) *Int J Hydrogen Energy* 1219:28
31. Iwakura C, Oura T, Inoue H, Matsuoka M (1996) *Electrochem Acta* 41(1):117
32. Iwakura C, Matsuoka M, Asai K, Kohno T (1992) *J Power Source* 335:38
33. Senoh H, Hara Y, Inoue H, Iwakura C (2001) *Electrochim Acta* 967:46
34. Sakai T, Miyamura H, Kuriyama N, Kato A, Ogura K, Ishikawa H (1990) *J Electrochem Soc* 795:137
35. Iwakura C, Senoh H, Morimoto K, Hara Y, Inoue H (2002) *Electrochem* 70 (1):2